X-Ray Imaging and Multiferroic Coupling of Cycloidal Magnetic Domains in Ferroelectric Monodomain BiFeO₃

R. D. Johnson,[1,2,*] P. Barone,[3] A. Bombardi,[4] R. J. Bean,[5] S. Picozzi,[3] P. G. Radaelli,[1]
Y. S. Oh,[6] S.-W. Cheong,[6] and L. C. Chapon[7]

[1]*Department of Physics, Clarendon Laboratory, University of Oxford, Oxford OX1 3PU, United Kingdom*
[2]*ISIS facility, Rutherford Appleton Laboratory-STFC, Chilton, Didcot OX11 0QX, United Kingdom*
[3]*Consiglio Nazionale delle Ricerche, Istituto Superconduttori, materiali innovativi e dispositivi (CNR-SPIN), 67010 L'Aquila, Italy*
[4]*Diamond Light Source, Harwell Science and Innovation Campus, Didcot OX11 0DE, United Kingdom*
[5]*C.M.M.P., Department of Physics and Astronomy, University College London, Gower Street, London WC1E 6BT, United Kingdom*
[6]*Rutgers Center for Emergent Materials and Department of Physics and Astronomy,*
136 Frelinghuysen Road, Piscataway 08854, New Jersey, USA
[7]*Institut Laue-Langevin, BP 156, 6, rue Jules Horowitz, 38042 Grenoble Cedex 9, France*

Magnetic domains at the surface of a ferroelectric monodomain BiFeO₃ single crystal have been imaged by hard x-ray magnetic scattering. Magnetic domains up to several hundred microns in size have been observed, corresponding to cycloidal modulations of the magnetization along the wave vector $k = (\delta, \delta, 0)$ and symmetry equivalent directions. The rotation direction of the magnetization in all magnetic domains, determined by diffraction of circularly polarized light, was found to be unique and in agreement with predictions of a combined approach based on a spin-model complemented by relativistic density-functional simulations. Imaging of the surface shows that the largest adjacent domains display a 120° vortex structure.

The seminal work of I. Dzyaloshinsky [1] on the relativistic origin of weak ferromagnetism in antiferromagnetic substances is intimately connected to various emergent physical phenomena in condensed matter. For example, in the Skyrmion lattice the very presence of antisymmetric exchange interactions [1,2] in a noncentrosymmetric crystal stabilizes the long period helical structure in zero magnetic field. Also, for some spin-driven ferroelectrics (multiferroics), the electric polarization is driven by noncollinear magnetic orders: the inverse Dzyalonshinskii-Moriya effect. In this case, a phenomenological formulation [3] shows that for cycloidal magnetic structures, i.e., spins rotating in a plane that contains the magnetic wave vector (k), the electric polarization (P) transforms as a product involving the magnetization density and its gradient, the so-called Lifshitz invariant of the form $P \cdot \lambda$, where $\lambda = (\nabla \cdot L)L - (L \cdot \nabla)L$, and L is the antiferromagnetic order parameter. In a complementary view, the magnetic polarity can be thought of as arising locally from spin current [4], as $\lambda = k \times (S_i \times S_j)$, where S_i and S_j are spins on adjacent sites. Like P, λ is a polar vector, and will be called magnetic polarity in the remainder.

In BiFeO₃, arguably the most studied multiferroic owing to room temperature magnetoelectric coupling [5], ferroelectricity is the consequence of an improper structural transition at $T_c \sim 1100$ K to the polar space group $R3c$. In bulk samples, the magnetic ordering transition occurs at $T_N \sim 640$ K. While the two do not coincide, the respective

order parameters are coupled through antisymmetric exchange; i.e., P drives the appearance of the inhomogeneous magnetization through a coupling term $\gamma \lambda P$, where γ is a coupling constant, a scenario originally proposed by Kadomtseva [6]. The magnetic structure can be described locally as canted G-type, but with a long period modulation (~ 620 Å) in the hexagonal basal plane [7]. Subsequent studies [8,9] determined that the modulation is cycloidal with the spins rotating in the (k, z) plane, where k can take the three symmetry-equivalent directions $k_1 = (\delta, \delta, 0)$, $k_2 = (\delta, -2\delta, 0)$ and $k_3 = (-2\delta, \delta, 0)$ in the hexagonal setting of the $R3c$ group (employed throughout), and $\delta = 0.0045$ at 300 K.

In this Letter, we study the magnetic domains at the surface of a millimeter-size single crystal of BiFeO₃ with a single ferroelectric (FE) domain. Using the high momentum and spatial resolution of synchrotron x-ray diffraction, combined with circular polarization of the beam, we determine the absolute rotation direction of the magnetization in individual magnetic domains, which are found to have the same magnetic polarity. The sign of γ is determined and compared to model Hamiltonian and *ab initio* calculations. The large domains observed appear to form vortex structures with a closure of the wave vector for three adjacent 120° domains.

Single crystals of several mm³ were grown from a Bi₂O₃/Fe₂O₃/B₂O₃ flux by slow cooling from 870 °C to 620 °C. A selected crystal was mechanically cut and polished perpendicular to the c axis and then annealed to

remove any induced strain. A piezoresponse force microscopy (PFM) of the polished face (not shown) indicated that the surface had a single FE domain, with the electrical polarization pointing down into the sample. We label this domain FE $\downarrow$, with the opposite polar domain labelled FE $\uparrow$. The synchrotron x-ray experiments were performed at Diamond Light Source (UK) on Beamline I16 [10]. A horizontally polarized beam with a flux of $\sim 10^{12}$ photons per second was delivered by a linear undulator and tuned to an energy of 5.8 keV, off resonance of chemical elements present in $BiFeO_3$. Circular polarization of the beam was achieved by transmission through a 100 μm-thick diamond phase-plate, reducing the incident flux by $\sim 40\%$. The diamond crystal was aligned to scatter near the (111) reflection in transmission. For a certain deviation of $\Delta\theta$ from the Bragg condition, the crystal behaves as a quarter wave plate giving circular light. The handedness of the light is determined by the sign of $\Delta\theta$, which was calculated by dynamical scattering theory, and confirmed through experimental calibration of the beam line by measuring the x-ray dichroism of a standard ferromagnet.

To prevent contamination of the magnetic signal by charge scattering from neighboring structural reflections (δ is extremely small), we focussed on magnetic satellites of the $N = (0, 0, 9)$ reflection, which is extinct by the presence of c-glide planes. Additionally, contamination from multiple scattering was fully eliminated by positioning the sample at an azimuthal angle $\phi = -170.0°$ with respect to [1,0,0]. Diffraction of $\lambda/2$ x rays was made negligible by employing up-stream harmonic rejection

mirrors. The magnetic signal was clearly identified using the full x-ray beam size (100 μm vertical $\times$ 350 μm horizontal) with linearly polarized light scanning in reciprocal space around the positions of the six satellites $N \pm k_1$, $N \pm k_2$, $N \pm k_3$, for various positions on the crystal surface. The high momentum resolution allows the full separation of the six satellites, shown in Fig. 1, in contrast to previous neutron experiments [8,9]. The beam size was subsequently reduced using slits to create a footprint of 50×50 μm^2 on the crystal surface. An image of the magnetic domains (Fig. 2) was then constructed by step-scanning the sample position with a step size of 50 ± 1 μm, recording the intensities of magnetic Bragg peaks $N + k_1$, $N + k_2$, $N + k_3$ using rocking-curve scans. This procedure lead to the identification of three large magnetic k-domains corresponding to k_1, k_2, and k_3, shown in Fig. 2, and to some smaller domains at the edges of the scanned surface and around a sizeable crystal imperfection in the center of the specimen. The three main domains are extremely large, reaching up to 500 μm in some directions. Note that the average penetration depth of the x-ray beam is 3.3 μm at this energy, placing a lower bound on the domain thickness. Despite the long period of the modulation (620 Å), this result indicates that each domain corresponds to several hundred magnetic periods. The real space directions of the wave vectors are shown in Fig. 2(b). It appears that the modulation of the magnetization follows a 120° vortex structure described by the path $k_1 \rightarrow k_3 \rightarrow k_2$ when rotating anticlockwise on the crystal surface.
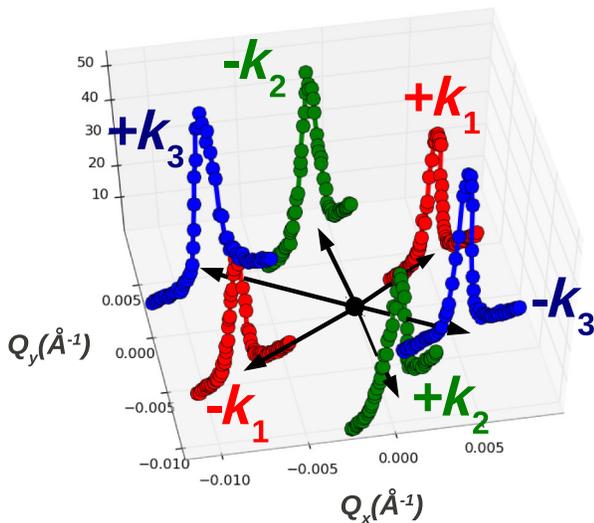

FIG. 1 (color online). Reciprocal-space scans showing magnetic Bragg intensities of the six satellites of the (0,0,9) parent reflection, with $k_1 = (\delta, \delta, 0)$ (red), $k_2 = (\delta, -2\delta, 0)$ (green) and $k_3 = (-2\delta, \delta, 0)$ (blue) and $\delta \sim 0.0045$. The x and y axis are taken, respectively, along the reciprocal a^* direction and real space b direction.
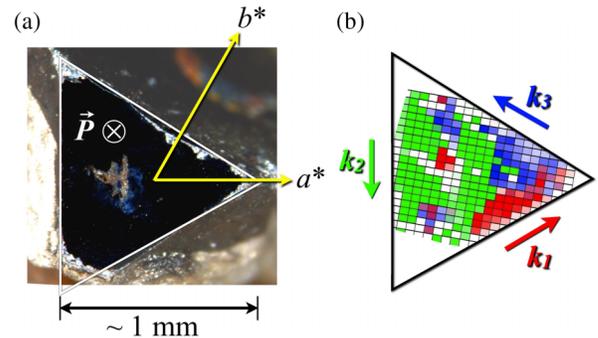

FIG. 2 (color online). (a) Photograph of the polished crystal surface of $BiFeO_3$ normal to the (001) axis (hexagonal setting, see text for details). A υ-shaped defect is seen in the center of the surface. The downward direction of the electric polarization $\boldsymbol{P}$ determined by PFM is shown (cross) together with the reciprocal a^*, b^* axis (yellow lines). (b) Distribution of antiferromagnetic domains with wave vectors $k_1 = (\delta, \delta, 0)$ (red), $k_2 = (\delta, -2\delta, 0)$ (green) and $k_3 = (2\delta, -\delta, 0)$ (blue). The direction of propagation of the cycloidal modulation in real-space coordinates for each domain is shown. Each pixel is colored according to the diffraction signal (domain) present. In the case of multiple diffraction peaks (overlap of domains), the pixels are shaded with mixed colors, respectively.

To determine the absolute rotation direction of the magnetization in each domain (magnetic polarity), scattering data were collected using circularly polarized light. For alternate chiralities of the x-ray beam (left- or right-handed), the intensities of the magnetic signals $N + k_1$, $N + k_2$, and $N + k_3$, were recorded after analysis with a pyrolitic graphite crystal as a function of the analyzer angle η, where $\eta = 0$ and $\eta = 90$ correspond to the σ' and π' polarization channels (perpendicular and parallel to the scattering plane), respectively. The incident-light polarization is described by the Stokes vector $\boldsymbol{P}_s = (P_1, P_2, P_3)$ [11], where P_1, P_2, P_3 represent respectively the degree of linear polarization along σ and π, oblique polarization ($\pm 45°$) and left or right circular polarization. P_1 and P_2 have been determined by fitting the variation with η of the Thomson scattering intensity for the reflection (0,0,6), taking into account the cross-channel leakage of the analyzer. $|P_3|$ was determined by supposing a fully polarized beam, i.e., $|P_3| = \sqrt{1 - P_1^2 - P_2^2}$. In our measurements, right and left handed light was 93% and 92% circularly polarized, respectively (see Supplemental Material [12] for the detailed calculations and conventions used). For each magnetic domain, the intensity (I_M) of the corresponding diffraction peak was evaluated using the density-matrix formalism [13],

$$I_M(\boldsymbol{Q}, \boldsymbol{P}_s, \eta) = \mathrm{tr}[D(\eta).V_m(\boldsymbol{Q}).\rho(\boldsymbol{P}_s).V_m(\boldsymbol{Q})^\dagger], \quad (1)$$

where ρ is the density-matrix representing the polarization of the incident beam, and D the matrix representing the analyzer configuration. $V_m = \boldsymbol{B}.\boldsymbol{M}(\boldsymbol{Q})$ is the scattering amplitude where $\boldsymbol{B}$ is expressed as a two by two matrix on the basis of the σ and π polarizations [11] and $\boldsymbol{M}(\boldsymbol{Q})$ the magnetic unit-cell structure factor. For the peaks at $\boldsymbol{Q} = (0, 0, 9) + \boldsymbol{k}_i (i = 1, 2, 3)$,

$$\boldsymbol{M}(\boldsymbol{Q}) = 6f(\boldsymbol{Q})[\boldsymbol{M}_\parallel - \beta i \boldsymbol{M}_z].e^{-i.18\pi z}, \quad (2)$$

where $f(\boldsymbol{Q})$ is the magnetic form factor for Fe^{3+}, calculated in the dipolar approximation from [14], $\boldsymbol{M}_\parallel$ and $\boldsymbol{M}_z$ are the magnetization vectors of the cycloid along $\boldsymbol{k}_i$ and the c-axis, respectively, and z is the fractional coordinate of Fe in the unit-cell ($z = 0.2208$ at 300 K). In our conventions $\beta = +1$ and $\beta = -1$ correspond to cycloids rotating counterclockwise (CCW) and clockwise (CW), respectively, when the structure is viewed propagating along $\boldsymbol{k}_i$ and c is up.

Comparison of intensities collected on the three main domains and calculations assuming circular cycloids (Fig. 3), unambiguously demonstrates that all magnetic configurations rotate CW following our definition. This is inferred from the η positions of the I_m extrema obtained with both light polarizations, which would be interchanged for a structure of opposite magnetic polarity. Within our conventions, $\boldsymbol{\lambda}$ is oriented in the $+c$ direction, antiparallel to $\boldsymbol{P}$. Refining the ellipticity of the cycloid ($\boldsymbol{M}_z/\boldsymbol{M}_\parallel$) does
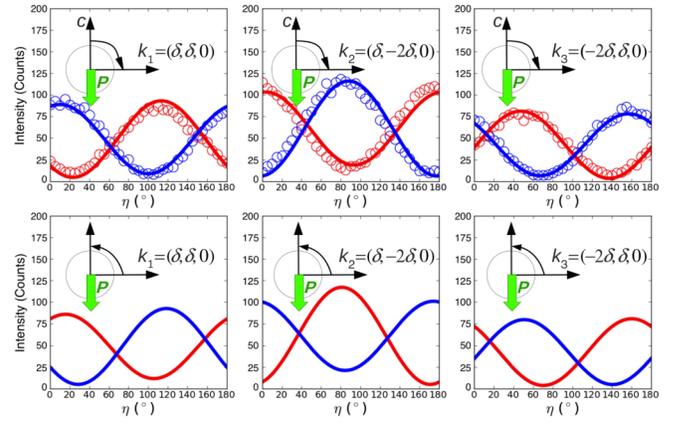

FIG. 3 (color online).   Top: Variation of the scattered x-ray intensity with the analyser angle η (circle symbols) for three magnetic reflections $(\delta, \delta, 0)$, $(\delta, -2\delta, 0)$, $(-2\delta, \delta, 0)$. The red (blue) color corresponds to the signal observed with a right-handed (left-handed) x-ray incident polarization. The solid lines show the results of a least-square refinement of the $BiFeO_3$ magnetic structure assuming $\beta = -1$ (CW, see text for details). Bottom: Calculated variation of the scattered x-ray intensity with the analyser angle η assuming $\beta = +1$ (CCW, see text for details). The direction of electric polarization $\boldsymbol{P}$ is shown as a green arrow.

not lead to significant improvements. This, and the failure to observe higher order magnetic satellites, supports the picture of a harmonic modulation at 300 K, discussed in [15,16]. No improvements of the fit were obtained by considering a slight tilt of the cycloidal plane, as recently suggested [17].

The relationship between ferroelectric and magnetic polarity was further investigated through *ab initio* spin-constrained calculations in the framework of density-functional theory (DFT). The VASP code [18] with the PAW pseudopotentials [19] was employed within the GGA + U approach [20,21] (U ranging between 3 and 7 eV and $J = 1$ eV for Fe d-states) including spin-orbit coupling, with a plane-wave cutoff of 450 eV. The total polarization was calculated via the Berry-phase formalism [22,23]. Structural parameters for the FE phase were taken from Ref. [24]. Due to its long periodicity, the true modulation of the magnetization is currently unaccessible to DFT. The modulation angle of the antiferromagnetic order parameter is given by $\theta = 2\pi(q_x x + q_y y)$, where $\boldsymbol{q} = \boldsymbol{k}_1$, $\boldsymbol{k}_2$, or $\boldsymbol{k}_3$. Choosing $\boldsymbol{q} = \boldsymbol{k}_3$, corresponding to a cycloidal modulation of spins rotating in the ac plane, one needs a supercell $na \times 2nb \times c$ in order to accommodate $\theta = 2\pi/na$. The largest possible supercell, $2a \times 4b \times c$, contains 240 atoms (just within the capabilities of state-of-the-art DFT simulations) and has modulation angle π/a. Accordingly, we considered a hypothetical spin configuration where the cycloidal period is reduced to two unit cells along a, with spins rotating CW (see Fig. 4, left panels) or CCW. The total energies of the two states are then compared in two symmetry-equivalent FE states with opposite
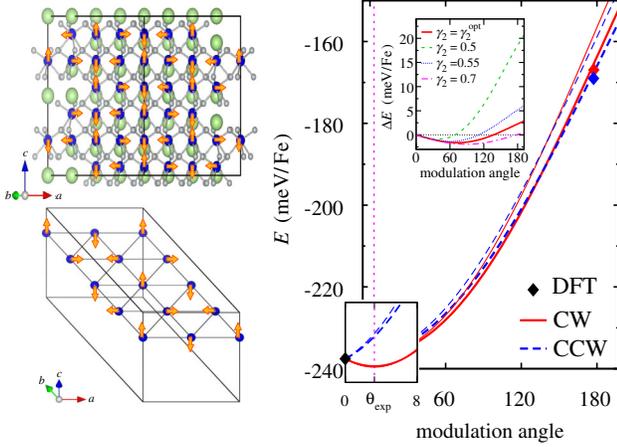
FIG. 4 (color online).   Sketch of the considered magnetic configuration in the $2a \times 4b \times c$ hexagonal cell of BiFeO$_3$. Upper left: side view. Bottom left: spin configuration for a selected layer of Fe ions. Right panel: mean-field energy as a function of the modulation angle for the FE ↓ domain, with all the parameters estimated from DFT with $U = 5$ eV (see text); vertical dotted line marks the experimental $\theta_{\exp}$, thick (thin) lines corresponds to total energy with (without) next-nearest neighbor contribution J_{NNN}. A zoom for small modulation angles is also shown. The inset shows the energy difference between CW and CCW configurations for the optimal γ, γ_2 and by artificially modifying the NNN contribution γ_2.

polarization, and in a reference paraelectric (centrosymmetric, $R\bar{3}c$) structure. As shown in Table I, the paraelectric state is degenerate with respect to magnetic polarity, which is then lifted in both FE states. Furthermore, the energy favored state switches when polarization is switched. The reliability of this trend has been checked for different values of U, as well as within a conventional local-density approximation, giving $|\Delta E|$ between 1.1 and 4.7 meV/Fe. These findings strongly point to a tight relationship between the magnetic polarity of the cycloidal modulation and the FE polarization. However, the rather large energy difference ΔE, as well as the disagreement of the predicted magnetic polarity with the experimental finding, are most probably due to the artificially short modulation of the magnetic configuration imposed in DFT calculations. Testing this hypothesis by mapping the energy evolution as a function of the modulation vector would require very demanding—if at all possible—DFT calculations. Instead, we adopted a different strategy as follows.

We introduce a Heisenberg-like spin model with nearest neighbor (NN) and next nearest neighbor (NNN) symmetric, as well as antisymmetric exchange interactions. The symmetric exchange interactions have been estimated by mapping the DFT energy of collinear ferro- and antiferromagnetic spin configurations onto the Heisenberg model, giving $J_{NNN}/J_{NN} \sim 0.03$, consistent with the value extrapolated from spin-wave dispersions [25,26]. The antisymmetric exchange interactions for a given direction of

TABLE I.   DFT results obtained for $U = 5$ eV, $J = 1$ eV. The energy difference is defined as $\Delta E = E_{CW} - E_{CCW}$. FE ↑ and FE ↓ are characterized by opposite collective displacements, τ, respectively upward and downward, of Bi sublattice with respect to O layers perpendicular to c axis.

	τ (Å)	P_c (μC/cm^2)	Δ E (meV/Fe)	Favored rotation
FE ↑	0.668	105.17	-2.34	CW
PE	0	0	0	...
FE ↓	-0.668	-105.17	2.34	CCW

P are captured through the magnetoelectric coupling constants γ (NN) and γ_2 (NNN weight). γ and γ_2 are then estimated by imposing the following constraints on the mean-field Heisenberg energy: i) the minimum of the energy occurs at the experimental modulation angle $\theta_{\exp} \sim 3.24°$ and ii) the energy difference at $\theta = \pi$ (i.e., the spin configuration simulated in our DFT calculations) is equal to ΔE, as evaluated from first principles. Under these assumptions we can estimate $\gamma \simeq 2.38 \times 10^{-4}$ V and $\gamma_2^{opt} = 0.6$, with $|\Delta E(\theta_{\exp})| \simeq 0.11$ meV/Fe, for $U = 5$ eV (the same order of magnitude was obtained for $U = 3$ eV and $U = 7$ eV). Following Ref. [6], the inhomogeneous magnetoelectric coefficient in the framework of Landau theory of phase transitions would be $\gamma = 4\pi A/lP_c \sim 5.8 \times 10^{-4}$ V (with exchange stiffness $A = 1.87 \times 10^5$ eV/cm [6], modulation period $l = 620$ Å and assuming the calculated $P_c = 105.17$ μC/cm^2), in good qualitative agreement with our estimate. Our model analysis also underlines the relevant role of NNN interactions, as through including J_{NNN} the mean-field Heisenberg energy almost reproduces the DFT results even at $\theta = \pi$, where the only constraint has been imposed on ΔE (Fig. 4). As anticipated, the energy-favored magnetic polarity appears to depend strongly on the modulation angle of the cycloidal configuration and on the relative weight of NN and NNN antisymmetric exchange interactions, which give rise to opposite energy contributions with a different dependence on θ (as detailed in the Supplemental Material [12]). For $\gamma_2 \lesssim 0.7$, the energetic competition between NN and NNN interactions causes the favored magnetic polarity to change sign when moving from short to long modulation periods, therefore reconciling DFT and experimental results.

In summary, magnetic domains of up to 500 μm have been observed at the surface of a single crystal of BiFeO$_3$ consisting of a single ferroelectric domain. The magnetic cycloids in each domain were found to propagate with a unique rotation direction imposed by the electric polarity of the crystal, in agreement with the predictions of our theoretical study if NNN interactions are taken into account. In future studies, it would be of interest to observe the switching of the rotation direction of the magnetic cycloids upon switching of the ferroelectric polarization by an applied electric field, as observed in TbMnO$_3$ [27], and predicted by our calculations.

---

*r.johnson1@physics.ox.ac.uk

[1] I. Dzyaloshinsky, J. Phys. Chem. Solids **4**, 241(1958).

[2] T. Moriya, Phys. Rev. **120**, 91 (1960).

[3] M. Mostovoy, Phys. Rev. Lett. **96**, 067601 (2006).

[4] H. Katsura, N. Nagaosa, and A. V. Balatsky, Phys. Rev. Lett. **95**, 057205 (2005).

[5] T. Zhao, A. Scholl, F. Zavaliche, K. Lee, M. Barry, A. Doran, M. P. Cruz, Y. H. Chu, C. Ederer, N. A. Spaldin, R. R. Das, D. M. Kim, S. H. Baek, C. B. Eom, and R. Ramesh, Nat. Mater. **5**, 823 (2006).

[6] A. Kadomtseva, A. Zvezdin, Y. Popov, A. Pyatakov, and G. Vorobev, JETP Lett. **79**, 571 (2004).

[7] I. Sosnowska, T. P. Neumaier, and E. Steichele, J. Phys. C **15**, 4835 (1982).

[8] D. Lebeugle, D. Colson, A. Forget, M. Viret, A. M. Bataille, and A. Goukasov, Phys. Rev. Lett. **100**, 227602 (2008).

[9] S. Lee, T. Choi, W. Ratcliff, R. Erwin, S.-W. Cheong, and V. Kiryukhin, Phys. Rev. B **78**, 100101 (2008).

[10] S. P. Collins, A. Bombardi, A. R. Marshall, J. H. Williams, G. Barlow, A. G. Day, M. R. Pearson, R. J. Woolliscroft, R. D. Walton, G. Beutier, and G. Nisbet, AIP Conf. Proc. **1234**, 303 (2009).

[11] F. de Bergevin and M. Brunel, Acta. Crystallogr. A **37**, 314 (1981).

[12] See Supplemental Material at http://link.aps.org/supplemental/10.1103/PhysRevLett.110.217206 for definitions and derivations of the x-ray scattering calculations, and details of the Heisenberg spin model.

[13] U. Fano, Rev. Mod. Phys. **29**, 74 (1957).

[14] P. J. Brown, *International Tables for Crystallography* (Springer, New York, 2006), Vol. C, p. 454.

[15] I. Sosnowska and R. Przeniosło, Phys. Rev. B **84**, 144404 (2011).

[16] M. Ramazanoglu, W. Ratcliff, Y. J. Choi, S. Lee, S.-W. Cheong, and V. Kiryukhin, Phys. Rev. B **83**, 174434 (2011).

[17] M. Ramazanoglu, M. Laver, W. Ratcliff, S. M. Watson, W. C. Chen, A. Jackson, K. Kothapalli, S. Lee, S.-W. Cheong, and V. Kiryukhin, Phys. Rev. Lett. **107**, 207206 (2011).

[18] G. Kresse and J. Furthmüller, Phys. Rev. B **54**, 11169 (1996).

[19] P. E. Blochl, Phys. Rev. B **50**, 17 953 (1994).

[20] J. P. Perdew, K. Burke, and M. Ernzerhof, Phys. Rev. Lett. **77**, 3865 (1996).

[21] S. L. Dudarev, G. A. Botton, S. Y. Savrasov, C. J. Humphreys, and A. P. Sutton, Phys. Rev. B **57**, 1505 (1998).

[22] R. D. King-Smith and D. Vanderbilt, Phys. Rev. B **47**, 1651 (1993).

[23] R. Resta, Rev. Mod. Phys. **66**, 899 (1994).

[24] A. Palewicz, I. Sosnowska, R. Przeniosło, and A. Hewat, Acta Phys. Pol. A **117**, 296 (2010).

[25] M. Matsuda, R. S. Fishman, T. Hong, C. H. Lee, T. Ushiyama, Y. Yanagisawa, Y. Tomioka, and T. Ito, Phys. Rev. Lett. **109**, 067205 (2012).

[26] J. Jeong, E. A. Goremychkin, T. Guidi, K. Nakajima, G. S. Jeon, S.-A. Kim, S. Furukawa, Y. B. Kim, S. Lee, V. Kiryukhin, S.-W. Cheong, and J.-G. Park, Phys. Rev. Lett. **108**, 077202 (2012).

[27] F. Fabrizi, H. C. Walker, L. Paolasini, F. de Bergevin, A. T. Boothroyd, D. Prabhakaran, and D. F. McMorrow, Phys. Rev. Lett. **102**, 237205 (2009).